Colloids and Surfaces B: Biointerfaces 177 (2019) 130–136

Contents lists available at ScienceDirect

Colloids and Surfaces B: Biointerfaces

journal homepage: www.elsevier.com/locate/colsurfb

Nanocrystalline diamond-based impedance sensors for real-time monitoring of adipose tissue-derived stem cells

Václav Procházka[a,b], Roman Matějka[c,d], Tibor Ižák[a,b,*], Ondrej Szabó[a], Jana Štěpanovská[a,d], Elena Filová[c], Lucie Bačáková[c], Vít Jirásek[a], Alexander Kromka[a,b]

[a] Institute of Physics, Czech Academy of Sciences v.v.i., Cukrovarnická 10, 162 00, Prague 6, Czech Republic
[b] Faculty of Electrical Engineering, Czech Technical University in Prague, Technická 2, 166 27, Prague, Czech Republic
[c] Institute of Physiology, Czech Academy of Sciences v.v.i., Videnska 1083, 14220, Prague 4, Czech Republic
[d] Faculty of Biomedical Engineering, Czech Technical University in Prague, nám. Sítná 3105, 272 01, Kladno, Czech Republic

ARTICLE INFO

Keywords:
Diamond film
Biosensor
Stem cells
Impedance spectroscopy

ABSTRACT

Cell-based impedance spectroscopy is a promising label-free method for electrical monitoring of cell activity. Here we present a diamond-based impedance sensor with built-in gold interdigitated electrodes (IDT) as a promising platform for simultaneous electrical and optical monitoring of adipose tissue-derived stem cells (ASCs). The impedance spectra were collected in a wide frequency range (from 100 Hz to 50 kHz) for 90 h of cell cultivation in chambers designed for static cultivation. Absolute impedance spectra were analyzed in terms of measured frequencies and cell properties monitored by a high-resolution digital camera. The control commercially-available impedance system, based on gold electrodes exposed to the cultivation media, and also our specially developed sensor with gold electrodes built into a diamond thin film detected three phases of cell growth, namely the phase of cell attachment and spreading, the phase of cell proliferation, and the stationary phase without significant changes in cell number. These results were confirmed by simultaneous live cell imaging. The design of the sensing electrode is discussed, pointing out its enhanced sensitivity for a certain case. The diamond-based sensor appeared to be more sensitive for detecting the cell-substrate interaction in the first phase of cell growth, while the control system was more sensitive in the second phase of cell growth.

1. Introduction

Bioelectrical sensors are of high interest as non-invasive label-free techniques for in vitro monitoring of biological events, due to their simplicity and fast response in real time. At the present time, there are two analytic approaches which employ either optical or electronic signal processing [1]. These two approaches have reached the state-of-the-art in a transducer type which converts a stimulus-induced cellular response into a quantifiable signal (i.e. a biosensor signal). Among the broad family of electronic systems, impedance measurement seems to be one of the simplest and most powerful methods for monitoring cellular signals during cell cultivation [2]. The main reason for its wide application is that the monitored impedance signal is sensitive not only to ionic currents but also to cell growth stages, i.e. cell attachment, spreading, shape, proliferation, differentiation and communication [3].

Diamond has been proposed as a promising material for life science and regenerative medicine due to its biocompatibility, chemical stability and favorable combination of optical, mechanical and electrical properties [4]. In addition, its surface can be covalently terminated by specific atoms or molecules which control cell occupation, adhesion, proliferation and cell differentiation [5]. In our previous studies, we have already introduced a surface-conductive diamond thin film as a functional layer in impedance sensors for biological studies [6,7] and for recognizing gas and chemical molecules [8,9]. It has been proven that intrinsic diamond thin film can be used as biocompatible biosensor for in-situ electronic (label-free) monitoring of cell behavior in cultures [6]. In that approach, the sensing principle of the diamond-based impedance sensor was based on impedance measurements, employing conductive hydrogen-terminated surface regions as in-plane electrodes that were separated by resistive oxidized surface regions. The thin diamond film was deposited on a glass substrate. This made it fully transparent in the visible range, including a low fluorescence background. Moreover, any possible and unwanted geometrical effects of metal electrodes (e.g. step edges) were avoided, and purely surface atom modifications defined and induced the p-type diamond surface conductivity [6]. Surface-conductive H-terminated diamond channels

* Corresponding author at: Institute of Physics, Czech Academy of Sciences v.v.i., Cukrovarnická 10, 162 00, Prague 6, Czech Republic.
E-mail address: izak@fzu.cz (T. Ižák).

https://doi.org/10.1016/j.colsurfb.2019.01.048
Received 8 November 2018; Received in revised form 22 January 2019; Accepted 23 January 2019
Available online 28 January 2019

were also applied in the case of solution-gated field effect transistors to study the interactions of human osteoblast-like SAOS-2 cells with a diamond surface [10].

In our present study, an impedance sensor with a functional diamond layer deposited on gold interdigitated electrodes is employed to monitor electrically and optically the growth activity of adipose tissue-derived stem cells (ASCs). ASCs were chosen because, together with human bone marrow mesenchymal stem cells, they had become the most popular adult stem cells used in tissue engineering, cell therapy and studies on cell differentiation towards various phenotypes [11]. For example, differentiation of ASCs towards adipocytes and osteoblasts was successfully quantitatively monitored in real time by impedance sensing [12]. Generally, cell differentiation is preceded by cell adhesion, spreading and proliferation, and these cell functions are also used for expanding the ASCs into desirable quantities for the purposes of further studies on various properties of these cells, and for their biomedical applications. In our study, we therefore focus on an investigation of cell adhesion, spreading and proliferation by impedance sensing with diamond-based impedance sensors. The results are compared with impedance measurements provided using a commercially-available gold interdigitated electrodes array (xCELLigence RTCA system, Roche Applied Science).

2. Experimental part

2.1. Preparation of sensors and measurement setup

The transducer of the sensor is formed by metal composite interdigitated electrodes (IDTs, 10 nm Ti and 80 nm Au) deposited on a quartz substrate (Corning XG, 15 × 15 mm^2 in size) (see Fig. S1a and S1b in the supplementary files). The width/gap of electrode periodicity was set to 100 μm. Samples with IDTs were coated with a diamond layer approx. 100 nm in thickness, using a linear antenna pulsed microwave plasma chemical vapor deposition system [13]. The deposition conditions were as follows: microwave power 2 × 1700 W, pressure 0.1 mbar, gas mixture 200/5/20 sccm of $H_2/CH_4/CO_2$, temperature 400 °C and process time 50 h. After deposition, the active sensor area was homogenously covered with a fully closed nanocrystalline diamond (NCD) film (Fig. S1c). The diamond character of the deposited film was confirmed by Raman spectroscopy [14].

Two types of sensors were used for the impedance measurements: gold IDT electrodes on glass (i) with a nanocrystalline diamond film, further labelled as “NCD sensor”, and (ii) without a nanocrystalline diamond film, further labelled as “Au sensor”. Before the experiments, the surface of the NCD sensors was oxygen-terminated using radio-frequency plasma. This step made the diamond surface hydrophilic and electrically insulating. To note, the surface of as grown diamond film is generally hydrogen-terminated due to high hydrogen content (> 88%) in the gas mixture used during deposition process. Hydrogen-terminated surface could lead to p-type surface conductivity. Therefore, to avoid any surface shortcuts and make the diamond surface well defined for cell cultivation, its oxygen-termination is needed.

The cells were cultivated in custom-built chambers designed for static cultivation (see Fig. S2b-S2d in supplementary files) in a 500 μl reservoir (made from polycarbonate) with a cultivation area of 7 × 10 mm^2. All materials that were used are biocompatible (nontoxic) to cells and are compatible with the autoclave sterilization process. The structure of the chambers is also optimized for real time microscopic imaging of the cells during their cultivation (Fig. S2a). During the experiments, the whole system was placed in an incubation chamber, where the temperature (37 °C) and the atmosphere (5% CO_2 and > 90% relative humidity) were kept constant. The impedance sensors were interconnected with a measuring device using gold spring connectors (Mill-Max Mfg. Corp., NY, USA). A custom multiplexer unit (MUX) was built to measure 8 parallel chambers during one experiment. Low-resistance reed relays were used (Littelfuse, Inc, IL, USA). The printed

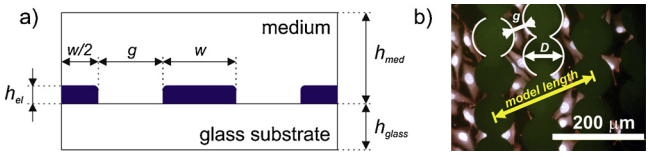

Fig. 1. a) Schematic draw of the computational domain used for FEM simulation. b) Representative fluorescence image of cells on xCELLigence sensor with highlighted dimensions of electrodes [6] (Note: the diameter (*D*) of circular-shape electrodes is ˜85 μm, and the gap (*g*) between electrodes with opposite polarity is ˜25 μm).

circuit board for MUX was optimized for equal length of traces for each channel to achieve similar impedance parameters.

The impedance parameters were measured using a Bode 100 (OMICRON electronics GmbH, Germany) vector analyser with custom built software for automated measurements of multiple channels. The impedance spectra were collected in a frequency range from 100 Hz to 50 kHz for 90 h cultivation. In this paper, we focus on impedance data measured at 1 kHz frequency.

Simultaneously with these experiments, reference measurements with the same cultivation conditions were performed using the xCELLigence RTCA system (Roche Applied Science) [3,15]. This system uses circular-shape Au IDT electrodes (Fig. 1b) and provides the time evolution of the so-called cell index, defined as $(Z_i\text{-}Z_0)/const$, where Z_i is the absolute impedance measured at time i and Z_0 is the starting impedance at time $t = 0$ s. Here, the measurement frequencies are limited to three discrete frequencies: 10 kHz, 25 kHz and 50 kHz.

2.2. Cell cultivation

Prior to cell cultivation, all parts of the cultivation chambers and impedance sensors were cleaned using 70% ethyl alcohol and were thoroughly rinsed with deionized water. Then the impedance sensor was installed in the cultivation chamber, and they were assembled all together (Fig. S2d). Finally, the assembly was sterilized using an autoclave (15 min at 121 °C) and was dried at 80 °C.

Human adipose tissue-derived stem cells (ASCs) were isolated from lipoaspirate obtained by liposuction [16]. The isolation was conducted in compliance with the tenets of the Declaration of Helsinki for experiments involving human tissues and under ethical approval issued by the Ethics Committee at the Bulovka Hospital in Prague (August 28, 2014). Written informed consent was obtained from the patient before the liposuction procedure. The cells in passage 2 were seeded on the impedance sensors and on the controls. The set contained eight cultivation chambers with 4x Au sensors and 4x NCD sensors. Here, 3 sensors from both the Au sensors and the NCD sensors were seeded with cells, while 1 sensor was left as the control (i.e. without cells), in order to investigate the influence of the culture medium, e.g. its evaporation and degradation over time. Pure and NCD-covered microscopic glass coverslips (both seeded with cells) were used as other control samples for a study of how the material of the sensor or the measurement itself affects the behavior of the cells.

The initial seeding density of ASCs was set according to refs. [17,18], and was adapted to the area of our designed culture chamber (0.7 cm^2) and the xCELLigence RTCA System (0.2 cm^2) (used for the reference measurements). The recommended density for RTCA is 3 000 cells/well (approx. 15 300 cells/cm^2), giving 11 000 cells/well for our home-made cultivation chamber. The cells were cultivated in standard high glucose Dulbecco's Modified Eagle's culture medium (DMEM) with the addition of 10% fetal bovine serum and human recombinant fibroblast growth factor-2 (FGF-2, 10 ng/ml). A 200 μl volume of the medium per well was applied in RTCA, and 650 μl per well was applied for our home-made cultivation chamber. After the cells had been seeded, the cultivation chambers equipped with sensors were connected to the MUX unit (Fig. S2), and time-lapse measurements began (i.e.

both electrical and optical monitoring). The measuring step period was set to 4 min.

After the impedance measurements, the cells were fixed using 4% paraformaldehyde and were fluorescence stained, using DAPI and phalloidin conjugated with tetramethylrhodamine (TRITC). The images of the fluorescently-stained ASCs on the impedance sensors and on controls were measured using a Leica DMi-8 microscope with a 10x objective and a Chroma multiband fluorescence filter.

2.3. FEM simulation

Finite element method (FEM) simulation using Comsol Multiphysics software was employed to study the distribution of the current density and the electric field for both the Au sensor and commercial xCELLigence RTCA system. For simplicity, in the first approach, the nanocrystalline diamond film was not taken into account, only the gold interdigitated electrodes with different width/gap periodicities deposited on glass substrates, and in the presence of a cell medium, were used for modelling in 2D geometry (see Fig. 1a). In the case of the xCELLigence system (circular electrodes), a perpendicular vertical cut along the centers of the circles was used as a computational domain (see "model length" in Fig. 1b). The other parameters were the same for both sensors, i.e. the height of the electrodes (h_{el}) 90 nm, the height of the glass substrate (h_{glass}) 100 μm, and the height of the cell medium (h_{med}) 200 μm. The height of the cell medium was chosen on the basis of the results of our first preliminary simulations, where we observed that higher values of h_{med} (≥200 μm) do not significantly affect the simulation results.

The conductivity of the cell culture medium (18.55 mS/cm) and the permittivity of water (80) were put as material properties in the finite element method model, as recommended in [19]. The specific electrical conductivity of gold was set to $\kappa = 49 \times 10^6$ S/m) [20]. For the glass substrate, conductivity 1×10^{-12} S/m and relative permittivity 4.2 were used.

In the FEM model, the time-harmonic equation of current continuity for the given AC frequency (1 kHz) was investigated, i.e. the investigated parameters are the amplitudes of the harmonic current and voltage forms. The voltage amplitude was set to 0.5 V. At the middle electrode the voltage was set to $U = U0*sin(\omega t)$, while at the edge electrodes $U = 0$ V.

3. Results and discussion

3.1. A comparison between the NCD sensor and the Au sensor

Fig. 2 summarizes the absolute and relative impedances measured by the pristine Au and NCD sensors (in the graphs labelled as 'Au' and 'NCD'), while the ASCs were being cultivated. The impedances are plotted for 1 kHz frequency. The as-measured absolute impedances for three NCD sensors and two Au sensors are plotted in Fig. 2a. Employing several sensors in a single experiment minimizes systematic errors and gives additional information about reliability and reproducibility of the sensors. For example, as can be seen in Fig. 2a, the absolute impedance values for the NCD sensors are approx. 2 times lower (˜300 Ω) than for the pristine Au sensors (˜600 Ω). This difference could be attributed to the character of the diamond layer. Generally, diamond is characterized as an insulating material. However, in the case of nanocrystalline diamond (NCD), the diamond film consist of small grains featured by the sp^3 carbon bonds (attributed to diamond) and the sp^2 carbon bonds (attributed to amorphous carbon) which are present at the grain boundaries. In the NCD films, sp^2 bonds dominate, making the diamond film less resistive [21]. In addition, the surface of a diamond film can exhibit p-type surface conductivity when it is finished by hydrogen atoms [6,22]. However, in our case we eliminated (minimized) this contribution while the surface was terminated by oxygen atoms using RF plasma, which is known as an insulating surface.

Further, we investigated the time evolution of the relative impedances as a function of sensor type (Fig. 2b). The relative impedances were calculated by subtracting the as-measured absolute impedances with Z_0 (i.e. Z_i-Z_0, where Z_0 is the impedance measured at time $t = 0$ s and Z_i is the impedance at time t_i). In Fig. 2b, the relative impedances measured for the medium with cells (Z_{cell}, solid lines) and without cells (Z_{medium}, dashed lines) for NCD sensors and Au sensors are plotted. Both Z_{medium} curves increased almost linearly, which could be attributed e.g. to the adsorption of proteins in the culture medium to the sensor surface. It has been reported that the adsorption of albumin, a major protein component of the serum supplement of the culture medium, can modulate the impedance, the electrical current and the potential of peptide-modified Au surfaces [23].

When Z_{medium} (the impedance measured for the medium without cells) is subtracted from Z_{cell} (the impedance measured for the medium with cells), we obtain in the first approximation of the impedance, which involves only the influence of cell cultivation. Side effects related to the ageing of the medium should be minimized [2] (see "baseline-corrected impedances" in Fig. 2c for one selected NCD sensor and for one Au sensor). These impedances are discussed below.

As can be seen in Fig. 2d, the time-dependent data of the baseline-corrected relative impedances can be divided into three main regions. At the beginning (up to 4 ÷ 6 h), there is a sharp increase of Z (region I). From 10 ÷ 12 h up to ˜60 ÷ 70 h (region II), the increase of Z is much slighter (the slope for this region is 10 ÷ 15 times lower than for region I). Finally, in region III at the end of the experiments (> 70 h), Z is almost constant or decreases slightly. Between these three main regions, we have defined two short intermediate regions. As was mentioned above, these data are plotted for 1 kHz frequency. However, the same behavior was also observed for impedance data measured at other frequencies. For example, Fig. S3a shows baseline-corrected impedances (i.e. Z_{cell}-Z_{medium}) for frequencies varying from 500 Hz to 20 kHz. As expected, the impedance decreases with increasing frequency. However, their time-dependent trends are almost the same (see the normalized impedance spectra in Fig. S3b). We therefore focus further on the impedance data interpretation measured at 1 kHz (Fig. 2d), especially on the explanation for the possible origins (causes) of regions I, II and III, also on the basis of the time-lapse optical images of the cells taken simultaneously during the experiments (Fig. 3).

The rapid increase in Z at the beginning (region I) seems to form a temporary period during which the cells were added to the cultivation medium, fell down onto the sensor active area, and started to adhere and spread on the substrate. Here, the shape of the cells was circular-like or ellipsoidal (see optical images in Fig. 3 (or in Fig. S4) from 0.5 h up to 3 h). From ˜4 h of the experiment, the first intermediate region began, in which the cells started to change their shape (Fig. 3). Most of the cells gained a spindle-like or polygonal morphology and formed numerous lamellipodia and filopodia. If the initial cell population density is enough low, i.e. if there is still reaming space between them on the sensor area, the cells proliferate quickly, causing a steep increase in Z (*cf.* Figs. 2d and 3 ; time from 6 h up to 15 h after cell seeding). Region II is characterized by a slighter increase in Z, which marks the formation of a confluent cell layer, accompanied by a slowdown of cell proliferation (*cf.* Figs. 2d and 3 ; from 17 h up to ˜65 h). Finally, region III (separated from region II with the second intermediated region) corresponds to cell confluence, i.e. full coverage of the active sensor area with cells. The cells stop their proliferation and their number is constant, or can even decrease slightly, due to their delamination from the surface, particularly from the Au surface (*cf.* Figs. 2d and 3 ; up to 90 h). Similar cell behavior was detected in NIH-3T3 fibroblasts cultured in a digital microfluidic system capable of impedance sensing [24], and also in mutant Chinese hamster V79 cells by an RT-CES system based on gold electrodes on silicon substrate [25], and operating on a similar principle similar to that of the xCELLigence system used in our present study.

In summary, the cell growth dynamics detected by our sensor

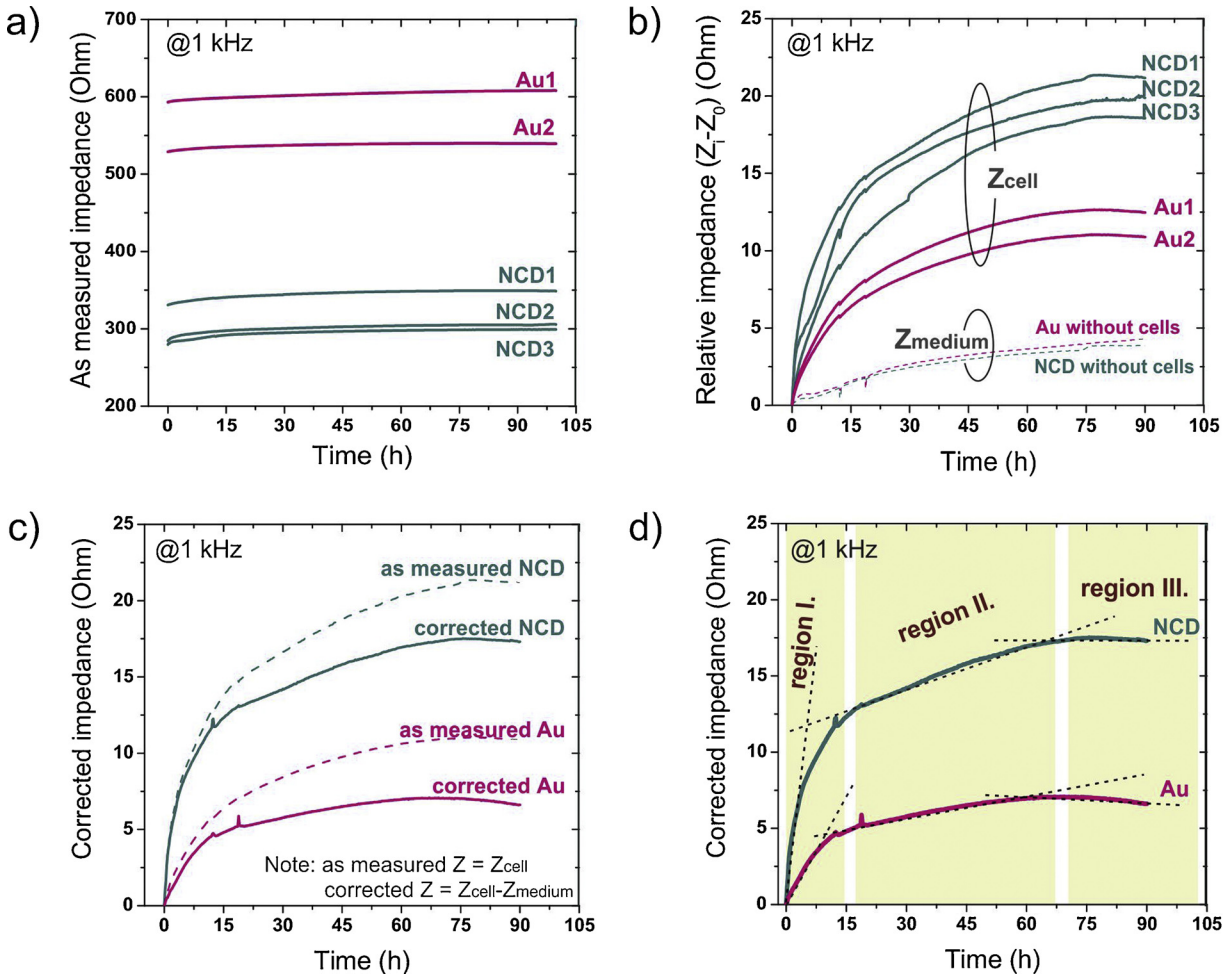

Fig. 2. a) As-measured absolute impedance, b) relative impedance and c),d) baseline-corrected impedance of adipose tissue-derived stem cells during the cultivation experiment, measured at frequency of 1 kHz for 4 days with diamond-coated and pristine Au IDT sensors (labelled as 'NCD' and 'Au', respectively). Notes: relative impedances represent shifted as-measured absolute impedances by Z_0 (impedance at time t = 0 s, i.e. Z_i-Z_0); baseline-corrected impedances are relative impedances subtracted by the impedances measured for medium without cells (i.e. Z_{cell}-Z_{medium}).

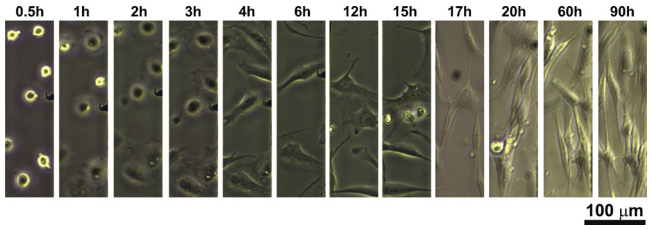

Fig. 3. Time-lapse optical images of cells on the NCD sensor surface during the cultivation and simultaneous electrical measurement.

resemble the classical "growth curves", which are widely used for evaluating the growth of cell populations. These growth curves consist of the following three major phases: the lag phase, in which the cells attach and spread on the cultivation substrate; the exponential phase, in which the cells proliferate; and the stationary phase, in which the cells reach confluence. Their numbers either do not change significantly or even decrease usually due to cell death and detachment [25–27]. The cell dynamics was also verified by direct cell counting in transparent regions of live cell-imaging pictures for the NCD sensor. The calculated time-dependent cell density on the NCD sensor is shown in Fig. S5a in the supplementary data. The resulting growth curve has standard cell growth behavior, consisting of three major phases: the lag phase, cell proliferation, and the stagnation phase. The cell growth curve, as will be discussed further, copies the cell index data of the xCELLigence sensor well (Fig. S5b). Note that the cell density data was obtained from time-lapse optical images of the cells on the surface of the NCD sensor; in the case of the xCELLigence system, real-time optical monitoring was not possible due to its specific structure, and just this simultaneous optical and electrical monitoring is the main advantage of our NCD sensor in comparison with commercial systems.

3.2. A comparison between the NCD sensor and the xCELLigence sensor

As has been mentioned above, simultaneously with the measurements performed by NCD and Au sensors, reference measurements were carried out using the commercially available xCELLigence RTCA system (i.e. by a gold interdigitated electrode array). Fig. 4a shows cell indexes measured by four xCELLigence sensors for the medium with cells (CI_{cell}, 2 blue and 2 green solid lines) and for the medium without cells (CI_{medium}, two red dashed lines). As in the impedance measurements taken by the Au sensors and NCD sensors, the cell indexes of the medium without cells were subtracted from the cell indexes of the medium with cells (i.e. the baseline-corrected cell index was calculated as $CI_{cell} - CI_{medium}$), and was compared with the impedance data measured by the NCD sensor (Fig. 4b).

As is shown in Fig. 4b, both plots consist of the three main regions described above. However, there are differences in slope steepness. While in the first region the slope is steeper for NCD sensor, in the second region the xCELLigence system shows steeper slope. It seems

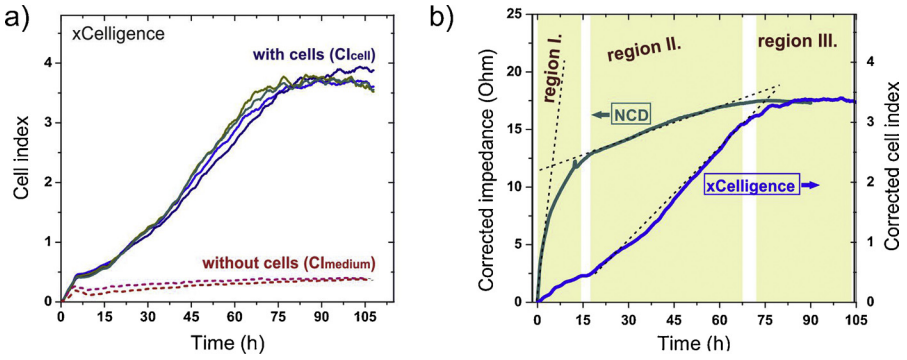

Fig. 4. a) Cell indexes measured by xCELLigence RTCA system for the medium with cells (CI_{cell}, blue solid lines) or without cells (CI_{medium}, red dashed lines). b) Comparison of baseline-corrected cell index (i.e. CI_{cell}-CI_{medium}, right y-axes) with baseline-corrected impedance (i.e. Z_{cell}-Z_{medium}, left y-axes) measured by xCELLigence RTCA system and NCD sensor, respectively (For interpretation of the references to colour in this figure legend, the reader is referred to the web version of this article).

that the NCD sensor is more sensitive that the xCELLigence system in the first region and less sensitive in the second region. Theoretically, the observed differences can be partially attributed to the different nature of diamond surface and gold/glass surfaces, and hence there are different cell adhesion properties in the early stage of cell cultivation, which could influence the impedance measurements. In our earlier studies and studies by other authors, NCD films have proved to be excellent substrates for cell adhesion [28,29], while Au is generally known to be rather bioinert. However, as shown in Fig. 2d, the NCD and Au sensors with the same IDT structures exhibit almost the same behaviors, so this explanation is not valid in our case. Another contribution is related to the different frequencies used during impedance measurements by the NCD sensor and by the xCELLigence system. However again, as shown in Fig. S3a and S3b (in the supplementary files), the frequency does not significantly influence the measurements for the NCD sensor.

Next, as shown in Fig. S5b, the cell growth curve, obtained from time-lapse optical images of cells on the NCD sensor surface, well copies the cell index data of the xCELLigence sensor. It is therefore supposed that the xCELLigence sensor should have similar cell growth curve. The difference in the impedance curves of NCD and xCELLigence sensors could be related to sizes of the IDTs. The NCD sensors and the xCELLigence RTCA system use different IDT structures. While for the NCD IDT sensor the width of the gap is the same as the electrode width (i.e. 100 μm, for example see Fig. S4), in the case of the xCELLigence IDT, the gap is much smaller than the electrode width. The width (or the diameter) of the circular-shape electrodes is 85 μm, and the gap between them is around 25 μm (Fig. 1b). This means that the ratio of the total electrode area to the gap area is 2:1 for the xCELLigence IDT and 1:1 for the NCD sensor.

The geometry of the IDT electrodes also influences the current density magnitude and its distribution over the sensor surface. Fig. 5 shows the distribution of the current density as simulated for two types of gold IDT electrodes on a glass substrate with 100/100 μm and 85/25 μm width/gap periodicity. The simulation predicts that for the xCELLigence sensor the maximum intensity of the current density is approx. twice as high as in the case of our Au IDT for the same AC voltage conditions.

The sensitivity distribution over the sensor surface is proportional to the relative current density. The regions of low current density will contribute less to the overall reduction in current (and therefore to the increase in impedance) when they are covered with cells. However, this will affect the sensitivity of the sensor by the same factor throughout the cell growth period.

Fig. 6 shows the current density distributions across the line between two electrodes at a Z-height of 1 μm. The current density peaks correspond to the electrode edges, with each peak having its half-width of half-maximum (HWHM) as indicated. Consequently, we can define the "sensitivity distribution ratio" (SDR) as

$$SDR = 4 \times HWHM \; / \; W_p \quad (1)$$

where W_p is the period width (the sum of the gap width and the electrode width). According to the simulation results, SDR is 0.052 for the Au IDT sensor and 0.073 for the xCELLigence system. In the first assumption the overall sensitivity of the two sensors is qualitatively comparable. However, differences in peak current density magnitudes may lead to different courses of Z_{medium}, as the electric properties of the medium are modified by the passage of the current. Indeed, as can be seen in the case of the xCELLigence sensor, Z_{medium} (CI) increases rapidly during the first 4 h, reaching 50% of its saturated value (see Fig. 4a). However, the increase in the Z_{medium} for the Au IDT sensor is much slower (compare with Fig. 2b). This may contribute to the steeper increase in the baseline-corrected impedance, as shown in Fig. 4b. However, the exact medium change mechanism is unknown in our case. More precise experimental measurement and simulation studies also need to be carried out in 3D geometry and taking into account the temporal and spatial change in the electrical properties of the medium + cells. However, this topic lies beyond the scope of present study.

Finally, 90 h after seeding, the cells reached confluence and were

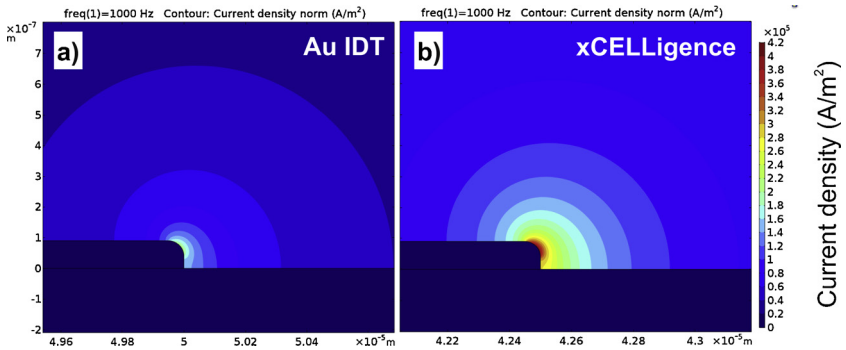

Fig. 5. Distribution of current density for Au IDT electrodes system (a) used for diamond deposition and for commercial xCELLigence sensor (b) plotted with the same scale bar.

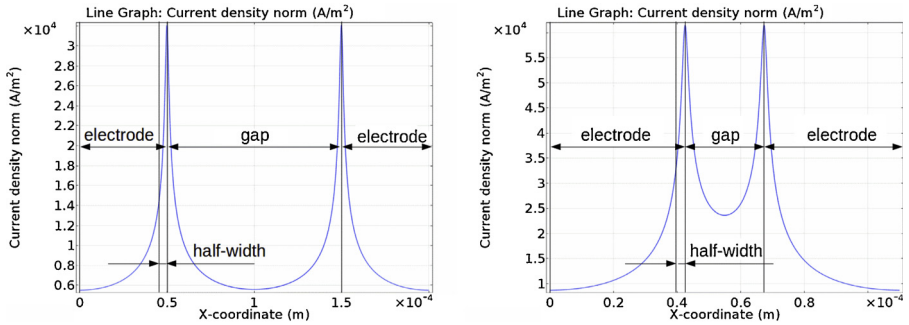

Fig. 6. Distribution of current density across the line located between electrodes of the Au IDT (left) and xCELLigence sensor (right) at 1 μm above the glass substrate.

homogenously distributed over the sensor area. Native pictures (Fig. S6 a–d in supplementary files) revealed that the cells were of spindle-shaped or polygonal morphology at the end of the experiments. Spindle-shaped morphology prevailed on the gold IDT sensor, while the polygonal morphology was more pronounced on the NCD-coated gold IDT sensor, and particularly on the NCD-coated and uncoated glass coverslips. The predominant spindle-shaped cell morphology could be a consequence of slightly delayed cell adhesion and spreading on the gold IDT sensor (Fig. 4b). It is generally known that gold surfaces are rather bioinert. For improved cell adhesion and growth, they should be further functionalized with chemical groups and/or biomolecules [30]. Nevertheless, the cells on all tested surfaces displayed a well-developed actin cytoskeleton (Fig. S6 e–h), as revealed by staining with TRITC-conjugated phalloidin, which binds filamentous (F) actin [31]. Generally, the microscopic observations of cell morphology proved that there were no significant differences between the gold IDT sensor, the NCD-coated gold IDT sensor and the control NCD-coated and uncoated glass surfaces. Also, the final cell population densities were similar on each tested surface (Fig. S6). These results are in good correlation with similar impedances and similar cell indexes detected by the gold IDT sensor and the NCD-coated gold IDT sensor in the interval of ˜75-90 h after cell seeding (Fig. 4b).

4. Conclusions

We have employed an impedance sensor type using a functional diamond layer deposited on metal interdigitated electrodes for monitoring the adhesion, growth and metabolic activity of adipose tissue-derived stem cells during cultivation. Wide frequency range measurements (100 Hz to 50 kHz) with time dependent impedance monitoring correlated with time-lapse optical microscopy enabled us to study the cell-cell and cell-substrate interactions and to investigate electrochemical processes at the electrode-electrolyte interface. The diamond-based sensor seems to be more sensitive during the early integration of cells with a diamond thin film (for cultivation time up to approx. 15 h after cell seeding), while the control commercially-available xCELLigence gold IDT system seems to be more sensitive in the later cell growth phase (for time interval from approx. 15 to 65 h after cell seeding). The simulated sensitivity distribution ratio rose more slowly for the Au IDT sensor than for the xCELLigence system, which is probably related to the steeper increase in its baseline-corrected impedance. However, the exact mechanism for these differences still needs further studies. We can conclude that the thin nanocrystalline diamond layer (100 nm) on the gold IDT provides a promising platform for future simultaneous electrical and optical monitoring of cell events on surfaces functionally terminated by various biomolecules.

Acknowledgments

This work was supported by the Ministry of Health of the Czech Republic (grant No. AZV 15-33018A), by CTU grant no. SGS17/136/OHK4/2T/13, and by Operational Programme Research, Development and Education financed by the European Structural and Investment Funds and the Czech Ministry of Education, Youth and Sports (Project No. SOLID21 - CZ.02.1.01/0.0/0.0/16_019/0000760). Mr. Robin Healey (Czech Technical University, Prague, Czech Republic) is gratefully acknowledged for his language revision of the manuscript.

Appendix A. Supplementary data

Supplementary material related to this article can be found, in the online version, at doi:https://doi.org/10.1016/j.colsurfb.2019.01.048.

References

[1] Y. Fang, Label-free biosensors for cell biology, Int. J. Electrochem. Sci. 2011 (2011) 1–16, https://doi.org/10.4061/2011/460850.
[2] Y. Xu, X. Xie, Y. Duan, L. Wang, Z. Cheng, J. Cheng, A review of impedance measurements of whole cells, Biosens. Bioelectron. 77 (2016) 824–836, https://doi.org/10.1016/j.bios.2015.10.027.
[3] N. Guan, J. Deng, T. Li, X. Xu, J.T. Irelan, M.-W. Wang, Label-free monitoring of T cell activation by the impedance-based xCELLigence system, Mol. Biosyst. 9 (2013) 1035, https://doi.org/10.1039/c3mb25421f.
[4] C.E. Nebel, B. Rezek, D. Shin, H. Uetsuka, N. Yang, Diamond for bio-sensor applications, J. Phys. Appl. Phys. 40 (2007) 6443–6466, https://doi.org/10.1088/0022-3727/40/20/S21.
[5] M. Verdanova, B. Rezek, A. Broz, E. Ukraintsev, O. Babchenko, A. Artemenko, T. Izak, A. Kromka, M. Kalbac, M. Hubalek Kalbacova, Nanocarbon allotropes-graphene and nanocrystalline diamond-promote cell proliferation, Small. 12 (2016) 2499–2509, https://doi.org/10.1002/smll.201503749.
[6] T. Ižák, K. Novotná, I. Kopová, L. Bačáková, B. Rezek, A. Kromka, H-terminated diamond as optically transparent impedance sensor for real-time monitoring of cell growth, Phys. Status Solidi B 250 (2013) 2741–2746, https://doi.org/10.1002/pssb.201300098.
[7] T. Izak, K. Novotná, I. Kopová, L. Bačáková, M. Varga, B. Rezek, A. Kromka, Hydrogen-terminated diamond sensors for electrical monitoring of cells, Key Eng. Mater. 605 (2014) 577–580, https://doi.org/10.4028/www.scientific.net/KEM.605.577.
[8] M. Davydova, M. Stuchlik, B. Rezek, K. Larsson, A. Kromka, Sensing of phosgene by a porous-like nanocrystalline diamond layer with buried metallic electrodes, Sens. Actuators B Chem. 188 (2013) 675–680, https://doi.org/10.1016/j.snb.2013.07.079.
[9] S. Stehlik, T. Izak, A. Kromka, B. Dolenský, M. Havlík, B. Rezek, Sensitivity of diamond-capped impedance transducer to tröger's base derivative, ACS Appl. Mater. Interfaces 4 (2012) 3860–3865, https://doi.org/10.1021/am3005829.
[10] T. Izak, M. Krátká, A. Kromka, B. Rezek, Osteoblastic cells trigger gate currents on nanocrystalline diamond transistor, Colloids Surf. B Biointerfaces 129 (2015) 95–99, https://doi.org/10.1016/j.colsurfb.2015.03.035.
[11] P.A. Zuk, The adipose-derived stem cell: looking back and looking ahead, Mol. Biol. Cell 21 (2010) 1783–1787, https://doi.org/10.1091/mbc.E09-07-0589.
[12] P.O. Bagnaninchi, N. Drummond, Real-time label-free monitoring of adipose-derived stem cell differentiation with electric cell-substrate impedance sensing, Proc. Natl. Acad. Sci. 108 (2011) 6462–6467, https://doi.org/10.1073/pnas.1018260108.
[13] Š. Potocký, M. Čada, O. Babchenko, T. Ižák, M. Davydova, A. Kromka, Perspectives of linear antenna microwave system for growth of various carbon nano-forms and its plasma study: perspectives of linear antenna microwave system, Phys. Status Solidi B 250 (2013) 2723–2726, https://doi.org/10.1002/pssb.201300085.
[14] V. Procházka, R. Matějka, T. Ižák, O. Szabó, J. Štěpanovská, L. Bačáková, A. Kromka, Real-time monitoring of stem cells by diamond-based impedance sensors, Proceedings 1 (2017) 515, https://doi.org/10.3390/proceedings1040515.
[15] F. Witzel, R. Fritsche-Guenther, N. Lehmann, A. Sieber, N. Blüthgen, Analysis of impedance-based cellular growth assays, Bioinformatics 31 (2015) 2705–2712, https://doi.org/10.1093/bioinformatics/btv216.

[16] M. Zhu, S. Heydarkhan-Hagvall, M. Hedrick, P. Benhaim, P. Zuk, Manual isolation of adipose-derived stem cells from human lipoaspirates, J. Vis. Exp. (2013), https://doi.org/10.3791/50585.
[17] K. Solly, X. Wang, X. Xu, B. Strulovici, W. Zheng, Application of real-time cell electronic sensing (RT-CES) technology to cell-based assays, Assay Drug Dev. Technol. 2 (2004) 363–372, https://doi.org/10.1089/adt.2004.2.363.
[18] J.Z. Xing, L. Zhu, J.A. Jackson, S. Gabos, X.-J. Sun, X. Wang, X. Xu, Dynamic monitoring of cytotoxicity on microelectronic sensors, Chem. Res. Toxicol. 18 (2005) 154–161, https://doi.org/10.1021/tx049721s.
[19] G. Blume, Electrical stimulation of NIH-3T3 cells with platinum-PEDOT-Electrodes integrated in a bioreactor, Open Biomed. Eng. J. 7 (2013) 125–132, https://doi.org/10.2174/1874120701307010125.
[20] E. Hering, K. Bressler, J. Gutekunst, Elektronik für Ingenieure und Naturwissenschaftler, Springer Berlin Heidelberg, Berlin, Heidelberg, 2014, https://doi.org/10.1007/978-3-642-05499-0.
[21] O.A. Williams, Nanocrystalline diamond, Diam. Relat. Mater. 20 (2011) 621–640, https://doi.org/10.1016/j.diamond.2011.02.015.
[22] A. Härtl, J.A. Garrido, S. Nowy, R. Zimmermann, C. Werner, D. Horinek, R. Netz, M. Stutzmann, The ion sensitivity of surface conductive single crystalline diamond, J. Am. Chem. Soc. 129 (2007) 1287–1292, https://doi.org/10.1021/ja066543b.
[23] H. Trzeciakiewicz, J. Esteves-Villanueva, R. Soudy, K. Kaur, S. Martic-Milne, Electrochemical characterization of protein adsorption onto YNGRT-Au and VLGXE-Au surfaces, Sensors 15 (2015) 19429–19442, https://doi.org/10.3390/s150819429.
[24] S.C.C. Shih, I. Barbulovic-Nad, X. Yang, R. Fobel, A.R. Wheeler, Digital microfluidics with impedance sensing for integrated cell culture andanalysis, Biosens. Bioelectron. 42 (2013) 314–320, https://doi.org/10.1016/j.bios.2012.10.035.
[25] J.Z. Xing, S. Gabos, B. Huang, T. Pan, M. Huang, J. Chen, High-throughput quantitative analysis with cell growth kinetic curves for low copy number mutant cells, Anal. Bioanal. Chem. 404 (2012) 2033–2041, https://doi.org/10.1007/s00216-012-6328-5.
[26] M. Toloudi, E. Ioannou, M. Chatziioannou, P. Apostolou, C. Kiritsis, S. Manta, D. Komiotis, I. Papasotiriou, Comparison of the growth curves of cancer cells and cancer stem cells, Curr. Stem Cell Res. Ther. 9 (2014) 112–116, https://doi.org/10.2174/1574888X0902140121163539.
[27] I. Kareva, G. Karev, From Experiment to Theory: What Can We Learn from Growth Curves? Bull. Math. Biol. 80 (2018) 151–174, https://doi.org/10.1007/s11538-017-0347-5.
[28] L. Grausova, L. Bacakova, A. Kromka, S. Potocky, M. Vanecek, M. Nesladek, V. Lisa, Nanodiamond as promising material for bone tissue engineering, J. Nanosci. Nanotechnol. 9 (2009) 3524–3534, https://doi.org/10.1166/jnn.2009.NS26.
[29] M. Amaral, A.G. Dias, P.S. Gomes, M.A. Lopes, R.F. Silva, J.D. Santos, M.H. Fernandes, Nanocrystalline diamond: *in vitro* biocompatibility assessment by MG63 and human bone marrow cells cultures, J. Biomed. Mater. Res. A 87A (2008) 91–99, https://doi.org/10.1002/jbm.a.31742.
[30] P.A. Santos, C.S. Rocha, M.S. Baptista, Adhesion and proliferation of HeLa and fibroblast cells on chemically-modified gold surfaces, Colloids Surf. B Biointerfaces 123 (2014) 429–438, https://doi.org/10.1016/j.colsurfb.2014.09.034.
[31] B. Chazotte, Labeling cytoskeletal F-Actin with rhodamine phalloidin or fluorescein phalloidin for imaging, Cold Spring Harb. Protoc. 2010 (2010), https://doi.org/10.1101/pdb.prot4947 pdb.prot4947-pdb.prot4947.